Estimation of scattering properties modifications caused by *in vivo* human skin optical clearing using line-field confocal optical coherence tomography

Sergey Zaytsev[1], Léna Waszczuk[2], Jonas Ogien [3], Arnaud Dubois[2], Walter Blondel[1], and Marine Amouroux[1]

[1]Universite de Lorraine
[2]Laboratoire Charles Fabry
[3]DAMAE Medical

August 28, 2024

Abstract

The image contrast and probing depth of optical methods applied to *in vivo* skin could be improved by reducing skin scattering using the optical clearing method. The aim of the present study was to quantify, from line-field confocal optical coherence tomography (LC-OCT) 3D images, the modifications of skin scattering properties *in vivo* during optical clearing. Nine mixtures of optical clearing agents were used in combination with physical and chemical permeation enhancers on human skin of three healthy volunteers. Scattering coefficient and anisotropy factor of the epidermis and the upper dermis were estimated from the 3D LC-OCT images of skin using an exponential decay model of the in-depth intensity profile. We were able to demonstrate a decrease in epidermal scattering (down to 33%) related to optical clearing with the best results obtained by a mixture of Polyethylene Glycol, Oleic Acid and Propylene Glycol.

Article type: Research Article

Estimation of scattering properties modifications caused by *in vivo* human skin optical clearing using line-field confocal optical coherence tomography

Sergey M. Zaytsev[1], Léna Waszczuk[2,3], Jonas Ogien[3], Arnaud Dubois[2,3], Walter Blondel[1], Marine Amouroux[1*]

[1] Université de Lorraine, CNRS, CRAN UMR 7039, Vandoeuvre-lès-Nancy, France, 54500

[2] Université Paris-Saclay, Institut d'Optique Graduate School, CNRS, Laboratoire Charles Fabry, Palaiseau, France, 91127

[3] DAMAE Medical, Paris, France, 75013

***Correspondence**

Marine Amouroux, Université de Lorraine, CNRS, CRAN UMR 7039, 54500 Vandoeuvre-lès-Nancy, France

Email: marine.amouroux@univ-lorraine.fr

Abstract

The image contrast and probing depth of optical methods applied to*in vivo* skin could be improved by reducing skin scattering using the optical clearing method. The aim of the present study was to quantify, from

line-field confocal optical coherence tomography (LC-OCT) 3D images, the modifications of skin scattering properties *in vivo* during optical clearing. Nine mixtures of optical clearing agents were used in combination with physical and chemical permeation enhancers on human skin of three healthy volunteers. Scattering coefficient and anisotropy factor of the epidermis and the upper dermis were estimated from the 3D LC-OCT images of skin using an exponential decay model of the in-depth intensity profile. We were able to demonstrate a decrease in epidermal scattering (down to 33%) related to optical clearing with the best results obtained by a mixture of Polyethylene Glycol, Oleic Acid and Propylene Glycol.

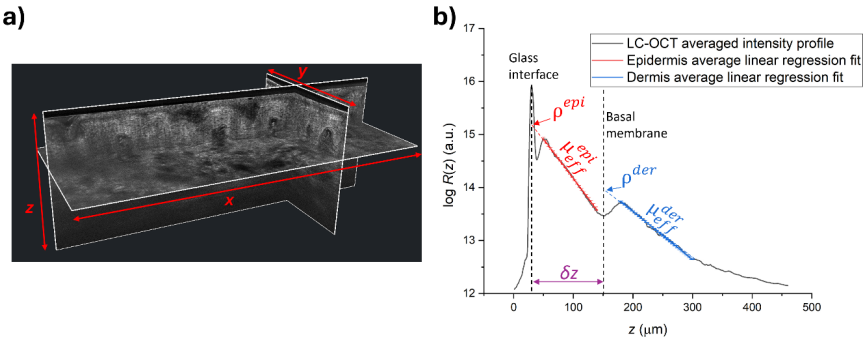

(a) 3D LC-OCT image of human skin *in vivo* , represented in slice view and (b) averaged intensity profile R (z), showing mean linear regression fit of each skin layer (epidermis – red, dermis – blue) and a corresponding pairs of observables (ρ^{epi}, $m_{\text{eff}}^{\text{epi}}$ andρ^{der}, $m_{\text{eff}}^{\text{der}}$). Dermal layer parameter ρ $^{\text{der}}$ deduced from the intercept with basal membrane (z = ˜150 µm) and corrected from epidermal layer attenuation.

Keywords: modelling; optical clearing; optical coherence tomography; optical properties, scattering; skin

Abbreviations: **CPE** , chemical permeation enhancer;**DMSO** , dimethyl sulfoxide; **LC-OCT** , Line-field Optical Coherence Tomography; **OA** , oleic acid; **OC** , optical clearing; **OCA** , optical clearing agent; **OCT** , Optical Coherence Tomography; **PEG** , polyethylene glycol; **PG** , propylene glycol; **RI** , refractive index; **SC** , stratum corneum;

1 INTRODUCTION

Human skin is an inhomogeneous organ comprised of three main layers: epidermis, dermis and adipose tissue. Each of these layers differs in thickness and morphology. Playing a role of an interface between the body and the environment, the skin performs physiological barrier function, protecting the body from ultraviolet rays, external physical impact and retaining water inside the body.[1]Since the skin is actively exposed to external irritants, it is susceptible to various pathological processes that can affect different layers of the skin, depending on the type and stage of the lesion. Due to the importance of the skin for the proper functioning of the body, the non-invasive diagnosis of skin diseases is an extremely important task, to which many studies are devoted. Optical methods based on the interaction of light with biological tissues have become a good potential addition or replacement to existing invasive methods (such as histopathological studies) due to their non-invasiveness, high sensitivity, the ability to obtain information in real time (without time consuming preparation of histological samples), as well as potential for clinical implementation.[2, 3]

Line-field confocal optical coherence tomography (LC-OCT) is a recently developed optical imaging method that combines the advantages of OCT and confocal microscopy, providing three-dimensional (3D) images of tissue with a quasi-isotropic resolution of ˜1 µm that is high enough to distinguish the cellular skin structure.[4,5] The applicability of LC-OCT to the diagnosis of skin diseases (including skin cancers) has been widely demonstrated.[6-8] Besides information on tissue morphology, the LC-OCT images also contain information on tissue optical properties. Since LC-OCT is an interferometric method, the image is obtained by registering low-coherence light backscattered or reflected by the tissue. This signal depends on three

main optical properties of the imaged tissue: absorption $\mu_a(\lambda)$ and scattering $\mu_s(\lambda)$ coefficients, which determine the fraction of light scattered or absorbed over a unit path length, respectively, and the scattering anisotropy factor $\gamma(\lambda)$ that is the mean cosine of scattering angles along the photon trajectory. The in-depth LC-OCT image intensity $I(z)$ depends on these optical properties and usually can be described (although only partially since the scattering anisotropy, for example, is not taken into account) by a Beer-Lambert law in the single-scattering regime:

$$I(z) \propto \exp^{-2m_t(\lambda)z}, \quad (1)$$

where z is depth in mm and $\mu_t(\lambda) = \mu_s(\lambda) + \mu_a(\lambda)$ is the total attenuation coefficient of the medium in mm^{-1}.[9] Those properties are determined by the size, density and shape of the tissue constituents (cells, collagen and elastin fibers, etc.). Assessing the optical properties of skin is critical for tissue characterization and quantification of structural changes associated with the pathological process.

The method most widely reported in the literature for extracting$\mu_t(\lambda)$ with conventional OCT techniques is to fit an exponential decay curve to the depth-dependent average intensity profile.[10] However, only few works were dedicated to separate assessment of scattering, absorption and scattering anisotropy from OCT images.[11] Such an assessment may allow one to obtain more comprehensive quantitative information about structural changes induced by a particular process in the skin than when estimating the integral $\mu_t(\lambda)$ coefficient. But this approach becomes complicated to implement when it comes to multilayered samples due to conventional OCT features and the concept of backscattered light as a fixed fraction of the attenuated light (which is assumed when extracting $\mu_t(\lambda)$ coefficient).[12] In contrast, a model based on Monte-Carlo simulations, developed by Jacques *et al* .[13] allows for a simple extraction of$\mu_s(\lambda)$ and $\gamma(\lambda)$ from focus-tracking OCT techniques and confocal microscopy. This model was validated on phantoms with pre-defined optical properties[14] and later applied to skin.[15] Since LC-OCT is a combination of OCT and confocal microscopy techniques, this technique is suitable for application of the aforementioned model. In her work, Waszczuk*et al* .[16] demonstrated that, with preliminary calibration using a phantom with known optical properties, it is possible to extract skin $\mu_s(\lambda)$ and$\gamma(\lambda)$ optical properties from 3D LC-OCT images of monolayered and bilayered phantoms.

However, the use of OCT (as well as other optical methods) for skin diagnosis is limited by strong light scattering in biological tissues, e.g., in skin. Scattering reduces the image contrast and resolution, lowering the possible diagnostic potential of such methods. This scattering originates from the inhomogeneities of skin layers (intralayer and interlayer inhomogeneities), leading to a mismatch in refractive indices (RI) between the tissue constituents and the interstitial fluid. To overcome this limitation, a tissue optical clearing (OC) method was proposed, based on the use of osmotic chemicals, called Optical Clearing Agents (OCA), whose RI was close to that of tissue solid material.[17,18] Being usually topically applied (but also can be injected into the tissue), OCA cause skin dehydration, followed by replacement the interstitial fluid with OCA and reversible collagen dissociation. It results in reduced scattering of treated tissue, leading to increased imaging depth and contrast.[19]

Translation of skin OC into clinical use, however, is connected with the need to comply with established regulations on the use of drugs, especially if the possible application will be performed on a lesional tissue. Since at pure concentrations OCA have been reported to have undesired side effects *in vivo* ,[20,21]their concentrations must be reduced in order to pass the threshold for clinical admission and biocompatibility.[22] But the low concentration of OCA does not allow to reach a sufficient clearing effect. To compensate for lower OCA concentrations in biocompatible applications, they can be used in conjunction with so-called chemical permeation enhancers (CPE), which are chemicals capable of temporarily disrupting skin barrier functions. The chemicals most commonly used as CPEs are alcohols,[23]dimethyl sulfoxide and fatty acids (Oleic acid).[24] There is also a large number of physical methods to enhance the skin permeability for OCA, such as microdermabrasion and therapeutic ultrasound,[25]which can be combined with CPE for a more efficient biocompatible effect of OCA.

Such possibility of *in vivo* clearing of human skin using biocompatible OCA concentrations has been ad-

dressed in our previous study,[26] where nine mixtures of one of three OCA compounds (Polyethylene Glycol (PEG), Sucrose and Glucose water solutions) in combination with one of three CPE compounds (Propylene Glycol (PG), Dimethyl sulfoxide (DMSO) and Oleic acid (OA)) were used with skin microdermabrasion and ultrasound to test their effectiveness in increasing LC-OCT in-depth image intensity and contrast. It was demonstrated that all tested OCA compositions caused an increase in the ratio between mean intensity and contrast extracted from 3D LC-OCT images. It was assumed that the main reason for such effects was a change in skin optical properties, i.e., a decrease of the scattering coefficient, caused by OCA. However, that assumption was not experimentally confirmed.

Taking into account the method developed by Jacques *at al* .[13], and later validated for the LC-OCT technique by Waszczuk *et al* .,[16] the goal of the current study was to quantify, using LC-OCT, the values of scattering coefficient $\mu_S(\lambda)$ and scattering anisotropy factor $\gamma(\lambda)$ and their modifications caused by *in vivo* biocompatible optical clearing of human skin.

2 MATERIALS AND METHODS

In this study, the composition of OCA compounds, the skin sites under investigation and the imaging modality was similar to our previously published work, where some complementary information could be found.[26]

2.1 Optical Clearing Agents and permeability enhancers

The choice of chemicals for this study was based on literature data on OCA currently used for human skin OC experiments.[17] Three chemicals from alcohol and sugar groups were used as OCA compounds: Polyethylene Glycol - 400 (PEG, Sigma-Aldrich, USA), 3M aqueous solutions of Sucrose (Sigma-Aldrich, USA) and Glucose (Sigma-Aldrich, USA). In order to satisfy the possible clinical admission requirements, OCA compounds did not exceed threshold of a concentration for topical application in the form of a solution, established by FDA. Thus, the data from FDA inactive ingredients database was used to fix the concentration of OCA mixture compounds, mentioned hereafter.[22] As there was no information about maximum concentration for glucose and sucrose solutions, a value (v/v) of 50% was established for the current study as it was previously reported as the most efficient one for OCT-assessed optical clearing.[27] To increase the *in vivo* efficiency of reduced concentrations of OCA compounds, they were mixed with three compounds with permeation-enhancing properties (CPE) from various chemical groups, such as alcohols, organic solvents and fatty acids: Propylene Glycol (PG, Sigma-Aldrich, USA), Dimethyl sulfoxide (DMSO, Sigma-Aldrich, USA) and Oleic acid (OA, Sigma-Aldrich, USA). Nine resulting mixtures of OCA and CPE and their corresponding compound concentrations are presented in **Table 1** . If it was not possible to mix OCA and CPE compounds only without exceeding FDA concentration thresholds, either complementary amount of distilled water or second CPE (namely PG) was added to the mixture. Additional information (such as the concentration threshold of each chemical used) can be found in our previous study.[26]

TABLE 1 . Nine mixtures of OCA and CPE with corresponding compounds concentrations (%, v/v) that meet the FDA-allowed concentration threshold.

OCA number	**OCA compound,** concentration (%, v/v)	**CPE compound, concentration (%, v/v)**	**Distilled water, concentration (%, v/v)**
1	PEG (3.52 %)	OA (7.44 %) + PG (89.04 %)	

2

PEG (3.52 %)

PG (92.48 %)

3

PEG (3.52 %)

DMSO (45.5 %) + PG (50.98 %)

4

Glucose (50 %)

OA (7.44 %) + PG (42.56 %)

5

Glucose (50 %)

PG (50 %)

6

Glucose (50 %)

DMSO (45.5 %)

4.5 %

7

Sucrose (50 %)

OA (7.44 %) + PG (42.56 %)

8

Sucrose (50 %)

PG (50 %)

9

Sucrose (50 %)

DMSO (45.5 %)

4.5 %

2.2 Technical equipment

2.2.1 LC-OCT

Detailed information on the LC-OCT device (DeepLive^{TM}, DAMAE Medical, France) used for image acquisition in this study can be found in[28]. Briefly, it is a Linnik interferometer-based imaging system with line illumination by supercontinuum laser at a central wavelength around 800 nm. A water-immersion microscope objective with a numerical aperture NA = 0.5 is incorporated in each arm of the interferometer. Backscattered spatially-coherent light is detected using a line camera. By in-depth scanning (along z -axis) during acquisition of horizontal section images with a field of view of 1.2 mm × 0.5 mm ($x \times y$), a stack of images can be compiled to obtain a 3D image of the tissue*in situ* with axial and lateral resolutions of less than 1.3 µm and a maximum penetration depth (z) of about 500 µm.

2.2.2 Physical permeability enhancers

Therapeutic ultrasound (Pulson 100, Gymna, Belgium) was used as a physical permeability enhancer as it allows to increase the skin permeability for OCA.[25] The duty cycle was 100%, the frequency 1 MHz and the power density 1 W/cm^2. Also, the skin microdermabrasion device (Philips VisaCare, Philips, Netherlands) was used. This procedure is commonly applied in cosmetology and involves the abrasion of stratum corneum (SC) layer that leads to increased penetration rate of OCA into the skin.

2.3 *In vivo* human skin sites

The experimental skin sites were the left and right hand thenar space dorsum of three healthy volunteers aged around 28 years with skin phototypes 2 and 3. An informed consent was obtained from the volunteers for topical OCA application, dermabrasion and sonophoretic treatment of experimental skin sites and the acquisition of 3D LC-OCT images. Volunteers' safety was guaranteed by FDA-approved concentrations of OCAs and by CE-marked LC-OCT, dermabrasion and sonophoresis medical devices. Since the dataset used in a current study had been acquired for the previously performed research,[26] an authorization for the human skin studies *in vivo* was obtained from the Saratov State Medical University Ethical committee (protocol 11 by June 7th 2022).

2.4 Optical clearing protocol

Ethanol-cleaned skin sites were subject to intact skin LC-OCT image acquisitions (t = 0 min). Then, after 1 minute of dermabrasion and image acquisition (t = 1 min, **Figure 1** (a)), one of OCA mixtures (˜100 µl) was topically applied and skin was exposed to therapeutic ultrasound twice for 5 minutes duration each (Figure 1(b)). Between and after ultrasound applications (t = 6 and 11 min, respectively), as well as for 30 minutes with 5 minute interval after manipulations were over (Figure 1(c)), LC-OCT imaging was performed (t = 16, 21, 26, 31, 36 and 41 min). Small amount of corresponding OCA was placed between the skin and the probe glass plate during image acquisitions to minimize parasitic reflections at the interface.

Control measurements were conducted at similar time points (t = 0 to 41 min) on the same skin site only subjected to paraffin oil as the LC-OCT probe immersion liquid (neither dermabrasion nor ultrasound were applied).

FIGURE 1 . Experimental *in vivo* human skin sites at different optical clearing experimental steps: (a) 1 minute of dermabrasion, (b) skin with topically applied OCA exposed twice to 5 minutes of sonophoresis, (c) LC-OCT image acquisition during entire experimental protocol.

2.5 Προcεccινγ οφ Λ˜-O˜T ιμαγεc το εcτιματεμ$_{\varsigma}$ ανδ γ φροµ cκιν λαψερc ιν ιο

2.5.1 Theoretical background of the model

More detailed explanation of the model proposed by Jacques *et al* . and later adapted for LC-OCT imaging system by Waszczuk *et al* . can be found in[13,16]. To estimate the optical properties of scattering media considering multiple forward scattering, the following modified exponential decay model of the depth-resolved reflectance $R(z)$, as proposed by Jacques *et al* .[13], was implemented:

$$R(z) = \rho \exp^{-2m_{\varepsilon\varphi\varphi} z}, \quad (2)$$

with

$$\begin{cases} m_{\text{eff}} = G(g, \text{NA})(m_a + a(g)\, m_s) \\ \rho = m_s \Delta \text{Zb}(g, \text{NA}) \end{cases}, \quad (3)$$

where ρ is the fraction of the light backscattered from the focus into the collection angle of the LC-OCT objective, $\mu_a(\lambda)$, $\mu_s(\lambda)$ and $g(\lambda)$ are the absorption, scattering and anisotropy coefficients, NA is the numerical aperture, ΔZ is the axial resolution of the imaging system, $G(g, \text{NA})$, $a(g)$ and $b(g, \text{NA})$ are the model parameters described in[13]. $G(g, \text{NA})$ takes into account the average photon path length considering the NA of the imaging system and the anisotropy factor g of the sample. For the LC-OCT setup used in this study, G was set to 1 (for NA = 0.5).[13] $a(g)$ reflects the possibility of photon to reach the focus in highly forward scattering media despite multiple scattering. For cases of isotropic scattering, $a(g)$ is close to 1, while for highly forward scattering medium $a(g)$ tends forward 0. This parameter describes the slowed down attenuation of light with depth by the so-called "serpentile phantoms".[16] 0 [?] $b(g, \text{NA})$ [?] 1 is the fraction of light that is scattered within the focus in such a way that it can be collected by the LC-OCT objective lens. It is ruled by the phase function of the sample and the numerical aperture of the imaging system.[13] The factor 2 in **Equation 2** accounts for the round-trip light attenuation by the sample. Since scattering in most biological tissue dominates over absorption ($\mu_s >> \mu_a$), the role of absorption was neglected in this study.[9]

2.5.2 Image processing algorithm to estimate μ_s and g values

The model described above assumed $\mu_{\epsilon\varphi\varphi}$ and ρ parameters as the experimental observables. Thus, to deduce optical properties (at the central wavelength $\lambda = 800$ nm of LC-OCT imaging system) $\mu_s(\lambda_{800})$ and $\gamma(\lambda_{800})$, the observables must be extracted from 3D LC-OCT images and then mapped to the model described by Equations 2 and 3. To do that, a mean intensity profile $I(z)$ (of a 0.8 mm × 0.3 mm ($x \times y$) central part of each individual horizontal section) over depth z of a 3D LC-OCT image (**Figure 2**) was calculated and then converted into reflectance $R(z)$ using relation $fI(z) = R(z)$. Calibration constant f can be obtained using double integrating spheres measurements on a calibration phantom.[13] In this work, the calibration phantom with known optical properties (estimated by the integrating spheres measurement as 4.6 mm^{-1} and 0.68 for μ_s and g, respectively) was kindly provided by Lena Waszczuk et al..[16]

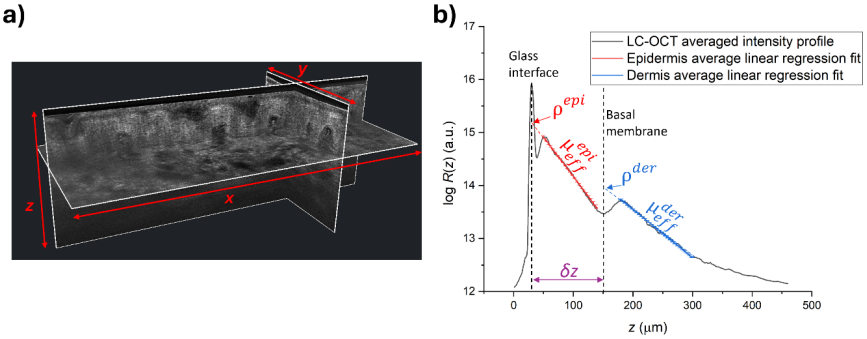

FIGURE 2 . (a) 3D LC-OCT image of human skin *in vivo*, represented in slice view and (b) averaged intensity profile $R(z)$, showing mean linear regression fit of each skin layer (epidermis – red, dermis – blue) and a corresponding pairs of observables (ρ^{epi}, $m_{\text{eff}}^{\text{epi}}$ and ρ^{der}, $m_{\text{eff}}^{\text{der}}$). Dermal layer parameter ρ^{der} deduced from the intercept with basal membrane ($z = \tilde{}150$ μm) and corrected from epidermal layer attenuation.

Then, a linear regression fit was applied separately to two parts of the intensity profile, corresponding to the epidermal and dermal layers (Figure 2(b)). Fitting areas were delineated manually for each layer, considering mostly linear parts of attenuation slope before the background of multiply scattered light becomes dominant and changes the slope.[13] μ_{eff} parameter of each layer ($m_{\text{eff}}^{\text{epi}}$ for epidermis and $m_{\text{eff}}^{\text{der}}$ for dermis)

was calculated as half of each linear fit slope. Epidermal $\rho^{\epsilon\pi\imath}$ parameter corresponding to the intercept of epidermal linear fit with depth $z = 0$, which is the interface between the LC-OCT probe glass surface and the skin surface. For the dermis, $\rho^{\delta\epsilon\rho}$ was obtained from $\rho^{\delta\epsilon\rho} e^{-2m^{\varepsilon\pi\imath}_{\varepsilon\varphi\varphi}\delta\zeta}$ (that is an intercept with between layer interface – basal membrane) by dividing it by correction factor $selectlanguagegreek e^{-2^{\mathrm{epi}}_{\mathrm{eff}}\mathrm{z}}$ (or by multiplying it with correction factor $e^{2m^{\varepsilon\pi\imath}_{\varepsilon\varphi\varphi}\delta\zeta}$) το ϛομπενσατε τηε αττενυα-τιον βψ τηε επιδερμαλ λαψερ οφ τηιϛκνεσς δz (Figure 2(b)).

Resulting experimental observables of each layer were then mapped to the model, described by Equations 2 and 3, using the following expression proposed by Jacques *et al* ., considering $\mu_{\mathrm{s}} >> \mu_{\mathrm{a}}$:[13]

$\underline{m_{\varepsilon\varphi\varphi}}$

$\mathrm{english}\rho = \frac{\mathrm{aG}}{b\Delta z}$ (4)

Such expression has the advantage of being independent from μ_{s} and depends only on wavelength, NA and g . With our experimental values $\lambda = 800$ nm and NA $= 0.5$, the anisotropy factor g of the corresponding layer was then retrieved as it is a function of μ_{eff}/ρ (as demonstrated in the works of Jacques and Waszczuk).[13,16] After retrieving g (λ_{800}) parameter, $\mu_{\mathrm{s}}(\lambda_{800})$ parameter can be calculated using Equations 2 and 3.

For each 3D image, a linear fit of each layer was repeated more than 100 times by scanning the fit limits by 10 μm with 1 μm step to estimate the variability of the fitting depending on the range chosen. Then, resulting kinetic changes of those parameters (in %) were averaged among volunteers with respect to timepoint of measurement and OCA mixture applied. This was done to make the observed changes more consistent as the initial values (intact skin measurements) are different between the volunteers due to interpatient variability.

3 RESULTS AND DISCUSSION

Scanning the manually established fit limits did not significantly affect the estimation of skin optical properties. The scattering coefficient $\mu_{\mathrm{s}}(\lambda_{800})$ mean standard deviation (SD) for all OCA and for all timepoints was only layer, respectively. The same values for the scattering anisotropy factor g (λ_{800}) were ˜0.05% and ˜5%. Thus, there was almost no influence of manual fitting range delineation on estimated optical properties.

Figure 3 shows the average of two LC-OCT intensity profiles R (z) before and after OC, together with the corresponding linear regression fits of the epidermal and dermal layers with the corresponding μ_{s} values. It can be seen from the round insets and the corresponding pixel intensity distributions that the image contrast and brightness from dermal layer (at 200 μm depth) is increased after optical clearing.

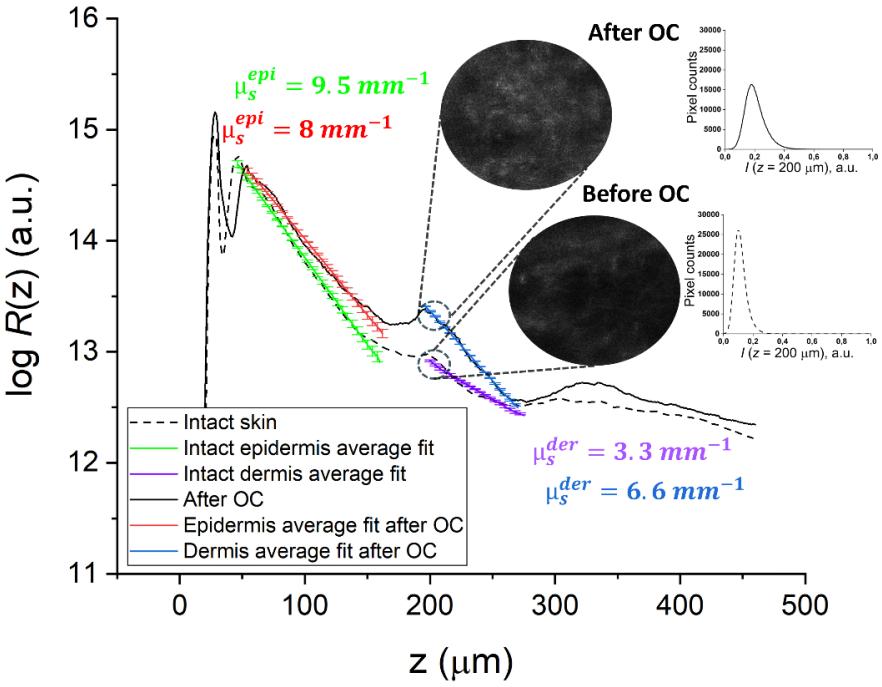

FIGURE 3 . Averaged skin LC-OCT intensity profiles$R\ (z\ )$ as a function of depth of one volunteer before (black dashed line) and after (black solid line) OC with mixture of Polyethylene glycol, Oleic acid and Propylene glycol with linear regression fit lines of epidermal and dermal layers and corresponding$\mu_{\ s}$ estimated values. Round insets display LC-OCT horizontal sections of dermal layer at 200 μm depth before (t = 0 min) and after OC (t = 11 min). The graphs next to the insets are the corresponding pixel intensity distributions.

Relative changes (in % of intact skin value) of scattering coefficientsm_s^{epi} and m_s^{der} (of epidermal and dermal layers, respectively) for the nine OCA and a control condition as a function of time are presented in **Figure 4** . Similar results, but for epidermal/dermal scattering anisotropy factor$g^{\text{epidermis}}$ and $g^{\text{dermis}}$are presented in **Figure 5** . SD bars that represent the variation between three volunteers vere removed from the graphs for the sake of clarity (due to strong overlapping between bars) and presented separately in **Table 2** (mean values over 10 timepoints) with respect to optical property, layer and OCA used.

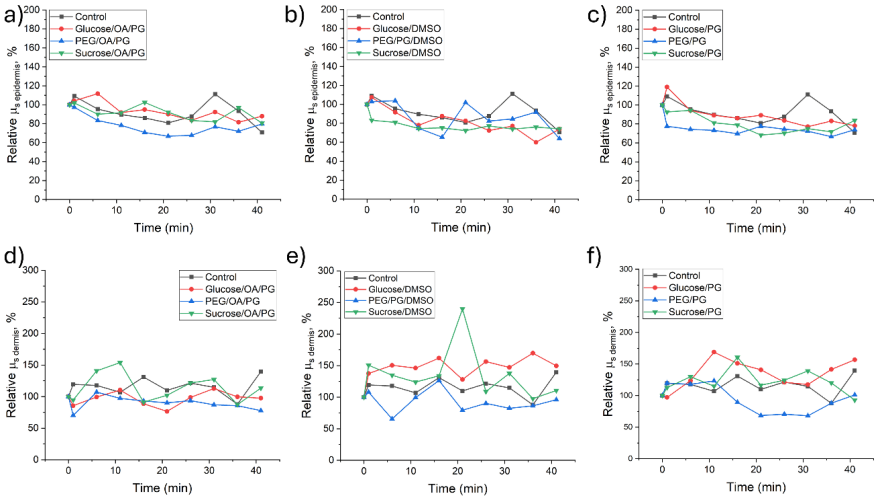

FIGURE 4 . Relative changes (expressed as % of intact skin value) of epidermal (a,b,c) and dermal (d,e,f) scattering coefficientm_s^{epi} and m_s^{der}, caused by the*in vivo* skin optical clearing protocol as a function of time (OA – oleic acid; PG - propylene glycol; PEG - polyethylene glycol; DMSO - dimethyl sulfoxide). Standard deviation bars were removed to keep data legible.

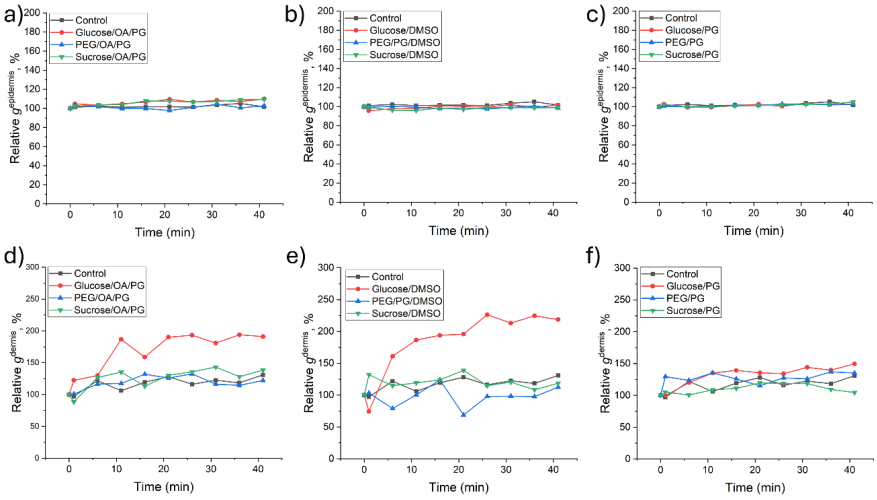

FIGURE 5 . Relative changes (expressed as % of intact skin value) of epidermal (a,b,c) and dermal (d,e,f) scattering anisotropy factor $g^{\text{epidermis}}$ andg^{dermis}, caused by the *in vivo* skin optical clearing protocol as a function of time (OA – oleic acid; PG - propylene glycol; PEG - polyethylene glycol; DMSO - dimethyl sulfoxide). Standard deviation bars were removed to keep data legible.

TABLE 2 . Mean standard deviation (SD, expressed as % of data) over 10 experimental time points representing the variation between three volunteers with respect to estimated optical property, skin layer and OCA used.

OCA mixture	**SD of m_s^{epi} (%)**	**SD of $g^{\text{epidermis}}$ (%)**	**SD of m_s^{der} (%)**	**SD of g^{dermis} (%)**
Control	25	3	24	30
PEG/OA/PG	9	6	26	21
PEG/PG	10	3	32	29
PEG/PG/DMSO	15	3	41	18
Glucose/OA/PG	11	6	16	81
Glucose/PG	11	5	24	40
Glucose/DMSO	10	2	50	123
Sucrose/OA/PG	22	5	43	41
Sucrose/PG	10	5	64	11
Sucrose/DMSO	12	1	42	22

Most of the curves related to the dermis optical properties show high standard deviation bars that are overlapped for the consecutive values (unlike the epidermis), thus hardening the interpretation of the observable kinetic changes (Figure 4 and 5 (d, e, f), Table 2). This is possibly due to the combined effect of measurement uncertainties propagated through the Jacques model. Additional reason might be the unstable LC-OCT probe positioning, which was constantly reapplied to tested skin sites without the possibility to use any kind of adhesive position-tracking labels due to mechanical manipulations with the skin surface in the beginning of the experimental protocol, making it impossible to analyze exactly the same tissue volume throughout the experiment. Another reason might be the morphological variation between the dermal layers

of the volunteers and a more significant contribution of multiple scattering to the dermal layer linear fit (as compared to epidermis).[16]

The uncertainties mentioned in the previous paragraph are described in detail in the work of Waszczuk *et al* .[16]First, there are uncertainties on the optical properties, estimated for a calibration phantom using double integrating spheres, which are then used in LC-OCT images processing. Second, there is an effect of both linear fit accuracy and variation between different images of the same sample on the μ_{eff} and ρ parameters. Finally, all these uncertainties affect the resulting LC-OCT estimation of scattering coefficient and scattering anisotropy factor. However, despite it was mentioned by Waszczuk *et al* . that when propagating through the model of Jacques the errors were amplified for high values of $\mu_s(\lambda_{800})$ and $\gamma(\lambda_{800})$, this method is still well suited to samples with relatively high scattering anisotropy ($\gamma(\lambda_{800})$ factor ranged between 0.7 and 0.9) and scattering coefficients $\mu_s(\lambda_{800})$ up to 12 mm^{-1}, i.e. biological tissues such as skin.

Epidermis scattering coefficient demonstrated ˜ 20% decrease for the control condition. But with a mean standard deviation over time of 25% of the observed values (Table 2) and the significant overlapping, it can be concluded that control conditions in general do not significantly affect the skin optical properties. However, it can also be seen that some OCA caused noticeable clearing effect in dermis. For example, a mixture of both sugars with DMSO caused a decrease in epidermis scattering m_s^{epi} (Figure 4(b)). Sucrose/DMSO mixture effect resulted into 28±18% decrease after 21 minutes of experimental protocol. Such decrease overcomes a moderate overall standard deviation (mean ˜12% for all timepoints). Mixture of Glucose and DMSO demonstrated more pronounced effect – 40±3% of epidermal scattering decrease (from 8.3 ± 1.3 mm^{-1} to 5 ± 0.9 mm^{-1} for three volunteers), which is greater than the mean variation of data over the time for this OCA – 10%. Both mixtures demonstrated as well an increase in scattering anisotropy of a dermal layer. However, as it was mentioned above and can be seen in Table 2, dermis values have a relatively high standard deviation, making it onerous to conclude that there is a clearing effect on dermis. So, only the general behavior can be mentioned. The result for Glucose/DMSO mixture is in a good agreement with observations made in our previous publication, where this mixture was considered as one of the most efficient among nine OCA in terms of in-depth increase of LC-OCT image intensity and contrast.[26] Such increase was assumed to be caused by the epidermis scattering decrease, that is quantitatively assessed in the present study. Other notable results are related to the mixtures of Glucose and PEG with PG as a permeation enhancer. Glucose/PG mixture (Figure 4(c)) caused 23% decrease of epidermal scattering with the mean ˜11% data variation over time and PEG/PG mixture caused 33% decrease with ˜10% mean data variation.

PEG/OA/PG mixture demonstrated the most pronounced m_s^{epi} decrease (Figure 4(a), blue triangle data points). Already after 21 minutes of experimental protocol (10 minutes after ultrasound-assisted clearing was over), this parameter decreased by 33 ± 17% for 3 volunteers, from 9.9 ± 1.1 mm^{-1}down to 6.6 ± 1.7 mm^{-1}. It can be seen that the decrease pattern in this case is the most confident among the other OCA. Moreover, for the first 6 measurement points (up to t = 21 min), the mean standard deviation is only ˜5% of the data (overall SD is ˜9% of the data). Considering all the mentioned uncertainties and high standard deviation bars in the case of other mixtures, PEG/OA/PG mixture demonstrated the most significant clearing effect. That is as well in good agreement with previous observations,[26] where PEG/OA/PG mixture demonstrated the best increase (40%) in image in-depth intensity and contrast after 10 minutes of ultrasound-assisted clearing.

Concerning the scattering anisotropy parameter, none of the OCA demonstrated significant changes in $g^{\text{epidermis}}$ with relatively low SD values. Together with decrease in m_s^{epi} one can conclude that OCA clearing effect on epidermis expressed and limited to matched RI of scattering particles and interstitial fluid. This RI matching effect is a well-investigated cause of reduction in tissue scattering mentioned in the literature.[17] On the contrary, dermal scattering does not change significantly due to high SD, but the tendency of dermal scattering anisotropy g^{dermis} towards increase indicates a different influence of tested OCA on skin dermis than to the epidermis *in vivo* . Mie theory explains that such behavior is related to an increase in the size of the scattering particles rather than to RI matching.[19] This applies to the dermis as there are bundles of collagen, which are probably swollen under the action of OCA mixtures, causing light to scatter in the forward direction.

Our results obtained on *in vivo* human skin demonstrate the possibility of LC-OCT quantitative estimation of changes in skin scattering coefficient $\mu_s(\lambda_{800})$ and scattering anisotropy factor $\gamma(\lambda_{800})$, caused by biocompatible optical clearing (involving the reduced concentrations of clearing agents used together with chemical and physical permeation enhancers). Moreover, the mixture of PEG/OA/PG has shown the best results. Although our current results were not validated with integrating spheres measurements (as the study was carried out on skin *in vivo*), this was done on phantoms in the study of Waszczuk*et al.* , demonstrating a good correlation between the values obtained using integrating spheres and application of Jacques' model to LC-OCT images.[16]

4 CONCLUSION

The experimental results presented in the paper demonstrate that the application of a model developed by S. Jacques to LC-OCT images makes it possible to quantitatively estimate the modifications in epidermal and dermal optical properties (scattering coefficient $\mu_s(\lambda_{800})$ and scattering anisotropy factor $\gamma(\lambda_{800})$ at the central wavelength $\lambda = 800$ nm of LC-OCT imaging system), caused by topically-applied biocompatible optical clearing, *in vivo.* The best results were obtained with the PEG/OA/PG mixture, whose application reduced scattering in the epidermis by $33 \pm 17\%$ already after the first external manipulations.

Different effects were observed for the two skin layers tested. In the epidermis, OC effect was mostly expressed in a reduction in the scattering coefficient, related to RI matching between scattering particles within the tissue and the interstitial fluid. In dermis, it was mostly related to the swelling of collagen fibers, causing an increase in the scattering anisotropy factor.

ACKNOWLEDGMENTS

This research was carried out with the support of the French National Research Agency (ANR) under the French PIA project "Lorraine Université d'Excellence" (ANR-15-IDEX-04-LUE). This study was part of the Spec-LCOCT project funded by the ANR (ANR-21-CE19-0056) and was carried with the DeepLive™ device of the PhotoVivo platform, which is part of the France Life Imaging (FLI) network and funded by Contrat de Plan Etat-Région Grand Est 2015-2020 (CPER IT2MP :*Innovations Technologiques, Modélisation et Médecine Personnalisée*) thanks to the financial support by European Regional Development Fund (FEDER), Grand Est Region and Ligue Contre le Cancer.

AUTHOR CONTRIBUTIONS

Sergey M. Zaytsev was involved in methodology, investigation, data processing and modelling, formal analysis, writing - original draft, review and editing. Léna Waszczuk was involved in data processing and modelling, writing – review and editing. Jonas Ogien was involved in writing – review and editing. Arnaud Dubois was involved in conceptualization, writing - review and editing, project management. Walter Blondel and Marine Amouroux were involved in conceptualization, methodology, formal analysis, writing – review and editing, project management. All authors have read and agreed to the published version of the manuscript.

CONFLICT OF INTEREST

The authors declare no financial or commercial conflict of interest.

DATA AVAILABILITY STATEMENT

The data that support the findings of this study are available from the corresponding author upon reasonable request.

REFERENCES

[1] T. B. Fitzpatrick, *Dermatology in general medicine* , Mcgraw-Hill Book Co., New York (1993).

[2] V. Narayanamurthy, P. Padmapriya, A. Noorasafrin, B. Pooja, K. Hema, A. Khan, K. Nithyakalyani, and F. Samsuri, "Skin cancer detection using non-invasive techniques", *RSC Adv* ., **8** (49), 28095–28130 (2018). doi: 10.1039/C8RA04164D.

[3] V. V. Tuchin, J. Popp, and V. Zakharov, *Multimodal Optical Diagnostics of Cancer* , 1st ed., Springer, Cham (2020).

[4] J. Ogien, A. Daures, M. Cazalas, J. L. Perrot, and A. Dubois, "Line-field confocal optical coherence tomography for three-dimensional skin imaging", *Front. Optoelectron.,* **13** (4), 381-392 (2020). doi: 10.1007/s12200-020-1096-x.

[5] A. Dubois, O. Levecq, H. Azimani, A. Davis, J. Ogien, D. Siret, and A. Barut, "Line-field confocal time-domain optical coherence tomography with dynamic focusing", *Opt. Express,* **26** (26), 33534-33542 (2018). doi: 10.1364/OE.26.033534.

[6] F. Latriglia, J. Ogien, C. Tavernier, S. Fischman, M. Suppa, J. L. Perrot, and A. Dubois, "Line-Field Confocal Optical Coherence Tomography (LC-OCT) for Skin Imaging in Dermatology", *Life,* **13** (12), 2268 (2023). doi: 10.3390/life13122268.

[7] M. Suppa, M. Fontaine, G. Dejonckheere, E. Cinotti, O. Yélamos, G. Diet, L. Tognetti, M. Miyamoto, C. Orte Cano, J. Perez-Anker, V. Panagiotou, A. L. Trepant, J. Monnier, V. Berot, S. Puig, P. Rubeghi, J. Malvehy, J. L. Perrot, and V. Del Marmol, "Line-field confocal optical coherence tomography of basal cell carcinoma: a descriptive study",*J. Eur. Acad. Dermatol. Venereol.,* **35** (5), 1099–1110 (2021). doi: 10.1111/jdv.17078.

[8] C. Ruini, S. Schuh, E. Sattler, and J. Welzel, "Line-field confocal optical coherence tomography—Practical applications in dermatology and comparison with established imaging methods",*Skin Res. Technol.* **27** (3), 340–352 (2021). doi: 10.1111/srt.12949.

[9] V. V. Tuchin, *Tissue Optics: Light Scattering Methods and Instruments for Medical Diagnosis* , 3rd ed., SPIE Press, Bellingham (2015). doi: 10.1117/3.1003040.

[10] S. Chang and A. K. Bowden, "Review of methods and applications of attenuation coefficient measurements with optical coherence tomography", *J. Biomed. Opt.* **24** (9), 090901 (2019). doi: 10.1117/1.JBO.24.9.090901.

[11] L. Thrane, H. T. Yura, and P. E. Andersen, "Analysis of optical coherence tomography systems based on the extended Huygens-Fresnel principle", *J. Opt. Soc. Am. A Opt. Image Sci. Vis.* **17** (3), 484–490 (2000). doi: 10.1364/josaa.17.000484.

[12] L. Thrane, M. H. Frosz, T. M. Jørgensen, A. Tycho, H. T. Yura, and P. E. Andersen, "Extraction of optical scattering parameters and attenuation compensation in optical coherence tomography images of multilayered tissue structures", *Opt. Lett.* **29** (14), 1641–1643 (2004). doi: 10.1364/OL.29.001641.

[13] S. L. Jacques, "Confocal Laser Scanning Microscopy Using Scattering as the Contrast Mechanism," in *Handbook of Coherent-Domain Optical Methods: Biomedical Diagnostics, Environmental Monitoring, and Materials Science* , V. V. Tuchin, Ed., 1157–1170, NY: Springer, New York (2013). doi: 10.1007/978-1-4614-5176-1_28.

[14] R. Samatham and S. L. Jacques, "Determine scattering coefficient and anisotropy of scattering of tissue phantoms using reflectance-mode confocal microscopy", *Proc. SPIE* ,**7187** , 152-159 (2009). doi: 10.1117/12.809684.

[15] N. Choudhury and S. L. Jacques, "Extracting scattering coefficient and anisotropy factor of tissue using optical coherence tomography," *Proc. SPIE* , **8221** , 144-148 (2012). doi: 10.1117/12.907401.

[16] L. Waszczuk, J. Ogien, F. Pain, and A. Dubois, "Determination of scattering coefficient and scattering anisotropy factor of tissue-mimicking phantoms using line-field confocal optical coherence tomography (LC-OCT)", *J. Eur. Opt. Soc.-Rapid Publ.* **19** (2), Art. no. 2 (2023). doi: 10.1051/jeos/2023037.

[17] V. V. Tuchin, D. Zhu, and E. A. Genina, *Handbook of Tissue Optical Clearing: New Prospects in Optical Imaging* , 1st ed., Routledge & CRC Press, Boca Raton (2022). doi: 10.1201/9781003025252.

[18] L. M. C. Oliveira and V. V. Tuchin, "Optical Clearing and Tissue Imaging," in *The Optical Clearing Method: A New Tool for Clinical Practice and Biomedical Engineering* , L. M. C. Oliveira and V. V. Tuchin, Eds., 107-138, Springer, Cham (2019). doi: 10.1007/978-3-030-33055-2_7.

[19] R. Samatham, K. G. Phillips, and S. L. Jacques, "Assessment of optical clearing agents using reflectance-mode confocal scanning laser microscopy", *J. Innov. Opt. Health Sci.* **3** (3), 183–188 (2010). doi: 10.1142/S1793545810001064.

[20] G. Vargas, A. Readinger, S. S. Dozier, and A. J. Welch, "Morphological Changes in Blood Vessels Produced by Hyperosmotic Agents and Measured by Optical Coherence Tomography", *Photochem. Photobiol.* **77** (5), 541–549 (2003). doi: 10.1562/0031-8655(2003)0770541MCIBVP2.0.CO2.

[21] V. V. Tuchin, A. N. Bashkatov, E. A. Genina, Yu. P. Sinichkin, and N. A. Lakodina, "In vivo investigation of the immersion-liquid-induced human skin clearing dynamics", *Tech. Phys. Lett.* **27** (6), 489–490 (2001). doi: 10.1134/1.1383834.

[22] "U. S. Food and Drug Administration, Inactive Ingredients Database", *FDA.gov* , Retrieved 12 February 2019, https://www.accessdata.fda.gov/scripts/cder/iig/index.cfm.

[23] Z. Zhi, Z. Han, Q. Luo, and D. Zhu, "Improve optical clearing of skin in vitro with propylene glycol as a penetration enhancer",*J. Innov. Opt. Health Sci.* **2** (3), 269–278 (2009). doi: 10.1142/S1793545809000590.

[24] Y. Liu, X. Yang, D. Zhu, R. Shi, and Q. Luo, "Optical clearing agents improve photoacoustic imaging in the optical diffusive regime",*Opt. Lett.* **38** (20), 4236–4239 (2013). doi: 10.1364/OL.38.004236.

[25] E. A. Genina, Y. I. Surkov, I. A. Serebryakova, A. N. Bashkatov, V. V. Tuchin, and V. P. Zharov, "Rapid Ultrasound Optical Clearing of Human Light and Dark Skin", *IEEE Trans. Med. Imaging* , **39** (10), 3198–3206 (2020). doi: 10.1109/TMI.2020.2989079.

[26] S. M. Zaytsev, M. Amouroux, V. V. Tuchin, E. A. Genina, and W. Blondel, "In vivo skin optical clearing efficacy quantification of clinically compatible agents using line-field confocal optical coherence tomography", *J. Biomed. Opt.* **28** (5), 055002 (2023). doi: 10.1117/1.JBO.28.5.055002.

[27] N. Sudheendran, M. Mohamed, M. G. Ghosn, V. V. Tuchin, and K. V. Larin, "Assessment of tissue optical clearing as a function of glucose concentration using optical coherence tomography", *J. Innov. Opt. Health Sci.* **3** (3), 169–176 (2010). doi: 10.1142/S1793545810001039.

[28] J. Ogien, C. Tavernier, S. Fischman, and A. Dubois, "Line-field confocal optical coherence tomography (LC-OCT): principles and practical use", *Italian Journal of Dermatology and Venereology* **158** (3), 171-9 (2023). doi: 10.23736/S2784-8671.23.07613-2.

Graphical Abstract

Line-field Confocal Optical Coherence Tomography (LC-OCT) is used to determine the human skin *in vivo* optical properties modifications caused by biocompatible optical clearing. After a prior calibration using a phantom with determined optical properties, a theoretical model is applied to mean in-depth intensity profiles of 3D LC-OCT images acquired during optical clearing protocol. As a result, kinetic relative changes of epidermal and dermal layer optical properties demonstrated with the best results caused by the mixture of Polyethylene Glycol, Oleic Acid and Propylene Glycol.

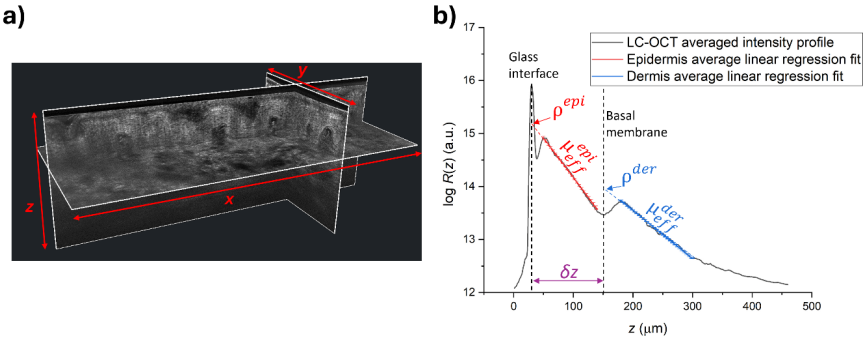

(a) 3D LC-OCT image of human skin *in vivo* , represented in slice view and (b) averaged intensity profile R (z), showing mean linear regression fit of each skin layer (epidermis – red, dermis – blue) and a corresponding pairs of observables (ρ^{epi}, $m_{\mathrm{eff}}^{\mathrm{epi}}$ andρ^{der}, $m_{\mathrm{eff}}^{\mathrm{der}}$). Dermal layer parameter ρ^{der} deduced from the intercept with basal membrane (z = ˜150 µm) and corrected from epidermal layer attenuation.